Analytical Methods

ROYAL SOCIETY OF CHEMISTRY

PAPER

View Article Online
View Journal | View Issue

Cite this: *Anal. Methods*, 2025, **17**, 1010

Ultrasensitive detection of methylene blue by surface-enhanced Raman scattering (SERS) with Ag nanoparticle-decorated magnetic CoNi layered double hydroxides†

Shuxian Ren, Jihong Fu, * Guoqi Liu, Haipeng Zhang, Boshen Wang and Junli Yu

The unreasonable use of organic dye leads to excessive residues in environmental water, which seriously threatens human health and the natural environment. In this paper, a spherical flower-like magnetic Fe_3O_4@CoNi layered double hydroxide@silver nanoparticle (Fe_3O_4@CoNi LDH@Ag NPs) SERS substrate was successfully fabricated *via* electrostatic self-assembly and applied for the sensitive detection of methylene blue (MB) in environmental water. The rapid concentration and separation of the SERS substrate from the water sample could be achieved using an external magnet. The Fe_3O_4@CoNi LDH@Ag NPs could not only rapidly enrich the trace analytes because of their outstanding absorptive capacity but also effectively enrich the cationic dye molecules to the "hot spots" through electrostatic interactions, resulting in higher SERS selectivity. Excellent SERS performance was observed, which exhibited a high enhancement factor (EF) of 5.81×10^8 and a low detection limit (LOD) of 1×10^{-11} mol L^{-1} with R6G as the probe molecule, and also possessed exceptional reproducibility and stability for at least 28 days. The Fe_3O_4@CoNi LDH@Ag NPs were used to detect MB, which displayed wide linearity (1×10^{-10} to 1×10^{-4} mol L^{-1}) and high recoveries (89.68–103.72%). This Fe_3O_4@CoNi LDH@Ag NP substrate offers easy separation and selective detection of cationic dyes, providing potential application for the detection of environmental contaminants.

Received 10th October 2024
Accepted 23rd December 2024

DOI: 10.1039/d4ay01841a

rsc.li/methods

1. Introduction

Organic dyes are indispensable colorants in the textile, printing, and dyeing industries; however, during the dyeing process, about 11–15% of the dyes are discharged into water together with industrial wastewater.[1] In recent years, with the increasing scale of industrial production, large quantities of wastewater containing toxic dyes have been illegally discharged into the environment, posing a serious threat to human health and the ecosystem. Methylene blue (MB) is a water-soluble heterocyclic compound widely used in the coloring of fabrics, leather and paper.[2] However, MB is toxic, carcinogenic and non-biodegradable, and when it enters the human body through the food chain, it can lead to respiratory distress, blindness and mental disorders.[3] Therefore, it is crucial to establish rapid, simple, and sensitive methods for detecting MB in environmental monitoring. So far, a variety of analytical methods have been used to detect MB, including ultraviolet spectrophotometry (UV),[4] chromatography-mass spectrometry,[5] and enzyme-linked immunosorbent assay.[6] These analytical methods have been widely used due to their inherent benefits of broad linearity, exceptional accuracy, and precision. Nevertheless, they have some drawbacks, such as exorbitant cost, long detection time, and complex sample pretreatment, limiting their further applications.

Surface-enhanced Raman spectroscopy (SERS) has emerged as one of the most promising spectroscopic techniques for detecting target compounds at low concentrations in environmental monitoring,[7] pharmaceutical analysis,[8] biomedical research,[9] and food safety[10] due to its high sensitivity, non-destructive detection, and good reproducibility. The SERS enhancement mechanisms are mainly categorized into electromagnetic enhancement (EM) and chemical enhancement (CM), with EM being dominant. EM mainly relies on the strong localized surface plasmon resonance (LSPR) of metal nanoparticles under excitation light, which is the main source of SERS enhancement.[11,12] The interstitial regions between neighboring metal nanoparticles are called "hot spots", which can further amplify the SERS signal. The successful implementation of SERS technology relies heavily on the development of the SERS substrate. In early SERS research, a noble metal sol substrate was mainly used, but single noble metal sol substrates are prone to agglomeration and have poor stability and

Key Laboratory of Oil and Gas Fine Chemicals Ministry of Education, Xinjiang Uyghur Autonomous Region, School of Chemical Engineering and Technology, Xinjiang University, Urumqi 830017, Xinjiang, China. E-mail: fjh.518@163.com

† Electronic supplementary information (ESI) available. See DOI: https://doi.org/10.1039/d4ay01841a

reproducibility.[13] Thus, to overcome the above-mentioned shortcomings, new materials have been combined with noble metal sols to prepare new substrates, which are receiving increasing attention. Singh *et al.* manufactured Ag–MoS_2 composite substrates *via* hydrothermal and wet chemical methods with a detection concentration of 5×10^{-9} mol L^{-1} for MB.[14] Ali *et al.* designed Zn_2GeO_4/Au *via* chemical vapor deposition for the rapid identification of MB with a detection limit of 1×10^{-4} mol L^{-1}.[15] However, the abovementioned methods have the disadvantages of low detection sensitivity and strict reaction conditions, which greatly limit their practical applications. Therefore, there is a pressing requirement to develop new SERS substrates with high detection sensitivity and mild preparation conditions.

Metal–organic frameworks (MOFs) are a type of porous materials that have gained significant interest recently because of their substantial specific surface area, convenient functionalization, and high porosity, making them potential SERS substrates to detect analytes in complicated environments.[16] For instance, Ge *et al.* prepared 3D Au/MOF-808(Zr) composites for the quantitative detection of the pesticide thiram in lake water.[17] Xu *et al.* developed FP/Ag/ZIF-8 as a substrate for the detection of thiram in lake water, peach juice, and apple peels using experimental filter paper.[18] However, although the fast development of MOF-based SERS substrates has created many new opportunities for SERS detection, there are still limitations. Firstly, the pore sizes of microporous MOFs are usually in the micropore range, which prevents the mass transfer of larger molecules into the pore system. Secondly, many MOFs have insufficient stability in water systems, which result in crystal structure collapse and lower mechanical strength. Therefore, the development of new SERS substrates with more accessible specific surface and high stability is still necessary.

Layered double hydroxides (LDHs) are a class of hydrotalcite compounds consisting of positively charged hydroxyl layers of divalent and trivalent metal ions, with the general formula $[M_x^{2+}M_y^{3+}(OH)_{2(x+y)}]A_{y/n}^{n-} \cdot mH_2O$ (M^{3+}: trivalent metal ions, M^{2+}: bivalent metal ions, and A: exchangeable anion).[19] Recently, LDHs, which can be synthesized by etching the MOF structure, have attracted particular attention because of their increased porosity, chemical affinity and specific surface area. Compared to MOFs, LDHs with a distinct ionic composition and hierarchical mesoporous structure can provide benefits such as decreased diffusion barriers and improved chemical and thermal stability, thus potentially enhancing the enrichment capacities. Some studies have been undertaken to investigate the possibility of SERS active composites made from LDH materials and noble metal nanostructures for use as SERS substrates. Zhao *et al.* constructed Ni–Fe LDH-covered Au nanoarrays as substrates for the fast and sensitive detection of gaseous styrene with a detection limit as low as 1 ppb.[20] Yang *et al.* synthesized an Ag NPs/ZnAl LDH hybrid system as a substrate, which exhibited an excellent SERS performance for 4-nitrobenzenethiol with a low detection limit of 1×10^{-10} mol L^{-1}.[21] These findings suggest that LDH-based substrates can drastically improve the SERS sensitivity, and thus demonstrate great potential to be widely used in detection using complex samples. To achieve high sensitivity, one feasible method is to improve the enrichment capacity of SERS substrates to adsorb more target molecules on the "hot spots" area by electrostatic interactions, π–π interactions and hydrogen-bonding. In addition, LDHs have a similar issue to other substrates in that they are difficult to separate from the matrix, which limits their practical use to some degree. Therefore, developing innovative magnetic LDH-based SERS substrates remains a challenging goal.

Herein, we successfully prepared a novel core–shell-flower-structured Fe_3O_4@CoNi LDH@Ag NP SERS substrate with Fe_3O_4 spherical nanoparticles as the core and ZIF-67 (ZIFs, MOF sub-class)-derived layered double hydroxide (LDH) as the shell (CoNi-LDH). The as-prepared Fe_3O_4@CoNi LDH@Ag NP SERS substrate exhibits excellent sensitivity, low limit of detection (LOD), high stability, good uniformity and reproducibility. The remarkable SERS performance of the Fe_3O_4@CoNi LDH@Ag NPs can be attributed to the following advantages: (i) magnetic Fe_3O_4, as the synthetic material, provides a quicker and more effective way to separate dye molecules from aqueous solution using a magnetic field; (ii) Fe_3O_4@CoNi LDH displaying positive charge is favorable for the dense immobilization of Ag NPs within the CoNi-LDH interlayer, which can generate a large number of "hot spots", and also effectively prevent the aggregation of Ag NPs; (iii) because of the electrostatic interactions between the Fe_3O_4@CoNi LDH@Ag NPs and dye molecules, the as-formed SERS "hot spots" show high selectivity to cationic dyes; and (iv) the ultrathin and porous structure improves the ability of Fe_3O_4@CoNi LDH@Ag NPs to absorb dye molecules. Therefore, the developed SERS substrate can realize the efficient, accurate and rapid detection of trace dyes in environmental water samples.

2. Methods and measurements

2.1 Material and reagents

Ferric chloride hexahydrate ($FeCl_3 \cdot 6H_2O$), methanol (CH_3OH), anhydrous ethanol (C_2H_5OH), methylene blue (MB), malachite green (MG), crystal violet (CV), Congo red (CR), tartrazine (TZ), and orange G (OG) were purchased from Xinbote Chemical Co., Ltd (Tianjin, China). Cobalt nitrate hexahydrate ($Co(NO_3)_2 \cdot 6H_2O$), anhydrous sodium acetate (NaAc), and ethylene glycol (EG) were purchased from Aladdin Biochemical Technology Co., Ltd (Shanghai, China). Polyethylene glycol was procured from Bailingwei Ultrafine Materials Co., Ltd (Hebei, China). Nickel nitrate ($Ni(NO_3)_2 \cdot 6H_2O$) was obtained from Xilong Scientific Co., Ltd (Guangdong, China). 2-Methylimidazole (2-MeIm) was obtained from McLean Biochemical Co., Ltd (Shanghai, China). Silver nitrate ($AgNO_3$) was obtained from Yongsheng Fine Chemical Co., Ltd (Tianjin, China). All chemicals were used Yongsheng Fine Chemical directly without further treatment.

2.2 Instruments

The morphology of the materials was characterized using a field emission scanning electron microscope (FE-SEM, SU8000,

Hitachi, Japan), and also a high-resolution transmission electron microscope (TEM) (JEM-2100F, JEOL Ltd, Tokyo, Japan) with energy-dispersive X-ray spectroscopy (EDS). UV spectra were recorded using a UV759 spectrometer (Shanghai Precision Scientific Instrument Co., Ltd, China). FT-IR spectra were recorded using a Vertex 70 (Bruker Co., Ltd, Germany). A vibrating sample magnetometer (VSM) (Lake Shore, USA) was used to determine the magnetic property of the substrate. The X-ray diffraction (XRD) patterns of the samples were recorded in the 2θ range of 5–80° using a Bruker D8 Advanced (Bruker Co., MA, USA). X-ray photoelectron spectroscopy (XPS) (Thermo Fisher, USA) was performed to study the surface element components in the substrate. Raman spectra were recorded using a Raman spectrometer (HORIBA Scientific, France) with a 633 nm laser.

2.3 Synthesis of Fe_3O_4

Fe_3O_4 nanoparticles were synthesized *via* the solvothermal method according to the reported method.[22] Briefly, $FeCl_3 \cdot 6H_2O$ (1.35 g) was dissolved in 40 mL ethylene glycol (EG), and then anhydrous sodium acetate (3.6 g) and polyethylene glycol (1 g) were added. After that, the mixed solution was stirred violently at 40 °C for 30 min. Subsequently, the mixed solution was transferred to a stainless steel autoclave (100 mL) and reacted at 200 °C for 10 h. After cooling to room temperature, the product was collected by centrifugation, and then washed with anhydrous ethanol and water alternately six times. Finally, the powder was dried under a high vacuum at 60 °C for 12 h.

2.4 Synthesis of Fe_3O_4@CoNi LDH

Firstly, Fe_3O_4 nanoparticles (2.5 mg), $Co(NO_3)_2 \cdot 6H_2O$ (1.4551 g), and 2-methylimidazole (0.4105 g) were ultrasonically dispersed in 40 mL methanol solution. After reaction for 12 h at room temperature, Fe_3O_4@ZIF-67 was obtained. Subsequently, 10 mg Fe_3O_4@ZIF-67 powder was ultrasonically dispersed in 10 mL anhydrous ethanol, and then 85 μL of Ni $(NO_3)_2 \cdot 6H_2O$ methanol solution (1.0 mol L^{-1}) was added dropwise. The mixture was transferred to a reactor and heated at 80 °C for 1 h. Finally, the power was washed three times with anhydrous ethanol and dried overnight at 60 °C in a vacuum to produce Fe_3O_4@CoNi LDH.

2.5 Synthesis of magnetic Fe_3O_4@CoNi LDH@Ag NP SERS substrate

Ag NPs were prepared according to a previous report.[23] $AgNO_3$ (8.5 mg) was dissolved in 50 mL ultrapure water, and then heated and stirred at 100 °C for 30 min. Subsequently, 2 mL of sodium citrate solution (1 wt%) was added, followed by reaction for 30 min to obtain Ag NPs. An easy electrostatic self-assembly technique was utilized to fabricate Fe_3O_4@CoNi LDH@Ag NPs. 5 mg Fe_3O_4@CoNi LDH powder was disseminated in 10 mL ultrapure water, and an equal volume of Ag NP solution was added. After ultrasonication for 10 min, the Fe_3O_4@CoNi LDH@Ag NPs were obtained. The Fe_3O_4@CoNi LDH@Ag NPs were directly mixed with the analyte as a substrate. The Fe_3O_4@CoNi LDH@Ag substrate combined the efficient adsorption ability of CoNi LDH and high superparamagnetic properties of Fe_3O_4.

2.6 SERS performance measurement

R6G solutions were made using ultrapure water at various concentrations of 1×10^{-11}, 1×10^{-10}, 1×10^{-9}, 1×10^{-8}, 5×10^{-7}, 1×10^{-7}, and 1×10^{-6} mol L^{-1}. The SERS performance of the Fe_3O_4@CoNi LDH@Ag NP substrate was evaluated using R6G (1×10^{-6} mol L^{-1}) as a probe molecule. After mixing R6G solution with the same volume of Fe_3O_4@CoNi LDH@Ag NPs (1 : 1, v/v) for 10 min, the SERS substrate was aggregated using an external magnet. Afterwards, the precipitate was transferred to a clean glass slide and tested directly. The SERS spectra were obtained in the range of 500 to 1750 cm^{-1}.

2.7 Preparation of actual samples

Three environmental water samples (snow water, rainwater, and lake water) were collected as actual samples. Centrifugation and filtration were used to remove sediment and grass debris from the water samples, which were then spiked to obtain samples containing 1×10^{-7}, 1×10^{-6}, and 1×10^{-5} mol per L MB. These solutions were mixed with the Fe_3O_4@CoNi LDH@Ag NP SERS substrate at a volume ratio of 1 : 1, and then aggregated with an external magnet. The precipitate was employed for the SERS analysis. The spectral data acquisition process for the actual sample is the same as that for the R6G standard solution.

3. Results and discussion

3.1 Characterization of Fe_3O_4@CoNi LDH@Ag NP SERS substrate

The process for the preparation of the Fe_3O_4@CoNi LDH@Ag NP SERS substrate is illustrated in Scheme 1. Firstly, Fe_3O_4 nanoparticles were synthesized *via* the solvothermal technique. Then, ZIF-67 were wrapped on the surface of the Fe_3O_4 nanoparticles by the coordination reaction using Co^{2+} and 2-MeIm. Secondly, after introducing Ni^{2+}, the H^+ generated by the hydrolysis of Ni^{2+} could etch ZIF-67, which generated the Fe_3O_4@CoNi LDH. Finally, Ag NPs were uniformly grown on the surface of Fe_3O_4@CoNi LDH through the electrostatic self-assembly method to fabricate Fe_3O_4@CoNi LDH@Ag NPs.

This research employed various characterization techniques to elucidate the structure and morphologies of Fe_3O_4, Ag NPs, Fe_3O_4@CoNi LDH and Fe_3O_4@CoNi LDH@Ag NPs (Fig. 1). Fig. 1a displays a representative SEM image of the Fe_3O_4 nanoparticles, which reveals that the synthesized Fe_3O_4 exhibits the typical spherical structure with a rough surface and average diameter of 320 nm. Fig. 1b shows the SEM image of the Ag NPs nanoparticles. It is evident that the Ag NPs displayed a spherical morphology with a smooth surface.

The SEM image of the Fe_3O_4@CoNi LDH (Fig. 1c) revealed that the prepared Fe_3O_4@CoNi LDH exhibited a spherical flower-like structure and composed of interconnected ultrathin layers with a thickness of subnanometer to several nanometers. Meanwhile, no spherical Fe_3O_4 particles were found, indicating

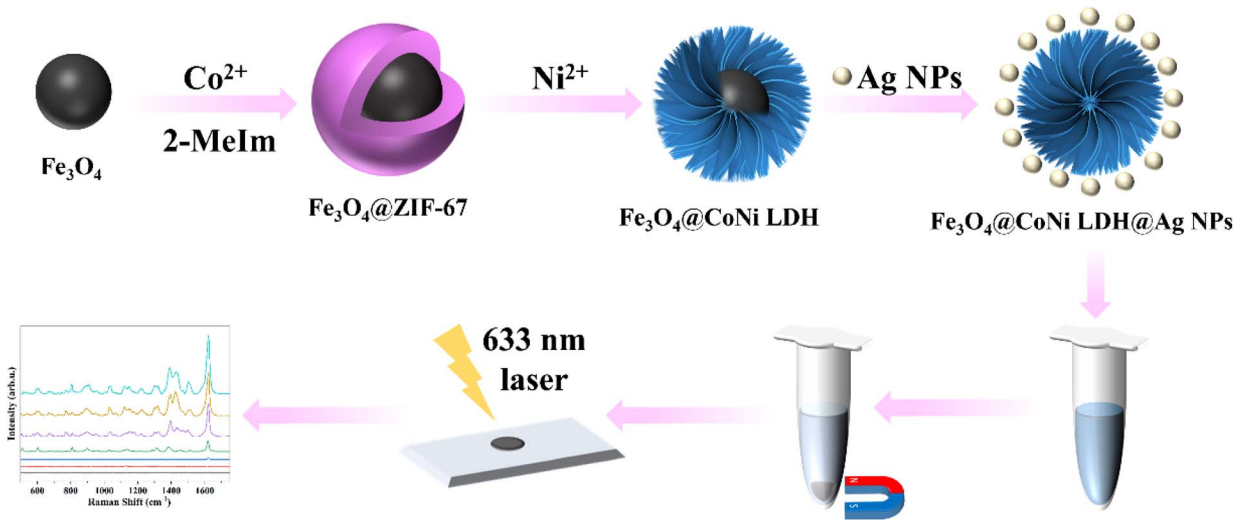

Scheme 1 Schematic of the preparation of the Fe_3O_4@CoNi LDH@Ag NP SERS substrate and the process used for SERS detection.

that the magnetic core was completely encapsulated by the CoNi LDH. The unique spherical flower-like morphology could efficiently improve the specific surface area and porosity of the material, which not only efficiently prevented the agglomeration of Ag but also offered more attachment sites for organic dyes. Furthermore, the Fe_3O_4 core could provide the product with the benefit of being easily separated from water.

According to the TEM image of Fe_3O_4@CoNi LDH@Ag NPs (Fig. 1d), a significant quantity of Ag NPs was densely distributed on the surface of the magnetic Fe_3O_4@CoNi LDH nanosheets, providing rich hotspots for the substrate and facilitating SERS enhancement. At the same time, the existence of Fe, Co, Ni, and Ag in the composite substrate was confirmed by the energy spectrum analysis. Fig. 1e–h show that strong Ag, Co, Ni and Fe signals were detected in the Fe_3O_4@CoNi LDH@Ag NPs. Co and Ni elements were uniformly distributed around Fe, which provided abundant positive charges for the substrate and conducive to the realization of electrostatic self-assembly between the substrate and the Ag NPs. Thus, the results strongly confirm the presence of Ag NPs on the surface of the Fe_3O_4@CoNi LDH nanosheets.

The FT-IR spectra of Fe_3O_4, Fe_3O_4@CoNi LDH, and Fe_3O_4@CoNi LDH@Ag NP composite SERS substrates are shown in Fig. 2a. In the spectrum of Fe_3O_4, the characteristic peak at

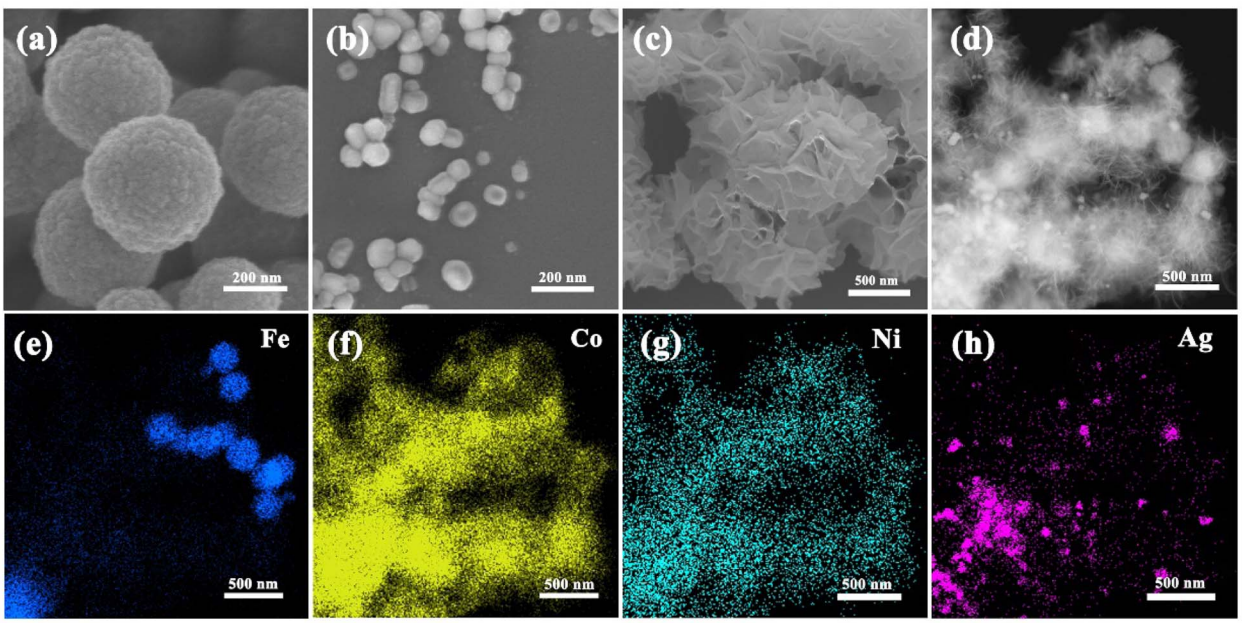

Fig. 1 SEM images of (a) Fe_3O_4, (b) Ag NPs and (c) Fe_3O_4@CoNi LDH; (d) TEM images of Fe_3O_4@CoNi LDH@Ag NPs; and (e–h) EDS elemental mapping spectra of Fe, Co, Ni, and Ag of Fe_3O_4@CoNi LDH@Ag NPs, respectively.

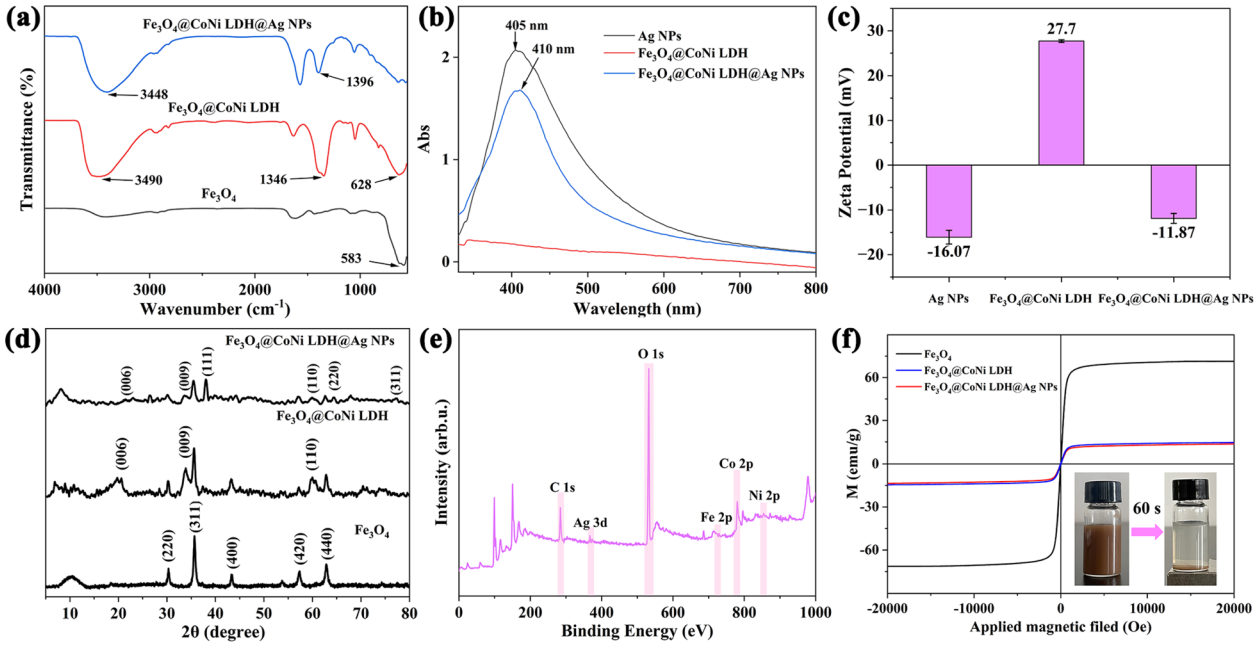

Fig. 2 (a) FT-IR spectra of Fe_3O_4, Fe_3O_4@CoNi LDH and Fe_3O_4@CoNi LDH@Ag NPs; (b) UV-visible absorption spectra of Ag NPs, Fe_3O_4@CoNi LDH and Fe_3O_4@CoNi LDH@Ag NPs; (c) zeta potentials of Ag NPs, Fe_3O_4@CoNi LDH, and Fe_3O_4@CoNi LDH@Ag NPs; (d) XRD patterns of Fe_3O_4, Fe_3O_4@CoNi LDH and Fe_3O_4@CoNi LDH@Ag NPs; (e) XPS survey of Fe_3O_4@CoNi LDH@Ag NPs; and (f) magnetic hysteresis loops.

583 cm^{-1} corresponds to the stretching vibration of Fe–O–Fe in Fe_3O_4.[24] In the spectrum of Fe_3O_4@CoNi LDH, the absorption peak at 628 cm^{-1} was attributed to the stretching vibration of Co–O and Ni–O, and the strong absorption peak at 1346 cm^{-1} corresponds to the N–O stretching mode of the surface adsorbed nitrate species, while the wide peak at 3490 cm^{-1} can be attributed to the hydroxyl stretching and bending vibration of the interlayer water molecules.[25] It is important to mention that the FT-IR spectrum of Fe_3O_4@CoNi LDH is highly similar to that of Fe_3O_4@CoNi LDH@Ag NPs, indicating that the loading of Ag NPs did not change the structure of Fe_3O_4@CoNi LDH and no chemical bond was formed between Ag NPs and Fe_3O_4@CoNi LDH in the composite.

The distinctive peaks of Ag NPs were not observed in the FT-IR spectrum of Fe_3O_4@CoNi LDH@Ag NPs. Thus, to further verify the existence of Ag NPs, the substrates were analyzed by UV-vis. Fig. 2b shows the UV-vis absorption spectra of Ag NPs, Fe_3O_4@CoNi LDH, and Fe_3O_4@CoNi LDH@Ag NPs. The absorption peak of Ag NPs was a broad peak located at 405 nm. Pure Fe_3O_4@CoNi LDH has no discernible peaks in the in the range of 350–800 nm. In comparison, the spectral band resulting from the localized surface plasmon shifted from 405 nm to 410 nm when Ag NPs were loaded on the surface of Fe_3O_4@CoNi LDH nanosheets. This may be due to the presence of Fe_3O_4@CoNi LDH affecting the dielectric environment around the Ag NPs, which led to changes in their characteristic peak shifts, indicating the successful preparation of the Fe_3O_4@CoNi LDH@Ag NP SERS substrate.

The zeta potential diagrams of Fe_3O_4, Fe_3O_4@CoNi LDH, and Fe_3O_4@CoNi LDH@Ag NPs are presented in Fig. 2c. Ag NPs and Fe_3O_4@CoNi LDH exhibited opposite charges of −16.7 and 27.7 mV, respectively, while the Fe_3O_4@CoNi LDH@Ag NPs were negatively charged with a zeta potential of −11.87 mV. These findings verified that the Fe_3O_4@CoNi LDH@Ag NPs were successfully created through the combination of Fe_3O_4@CoNi LDH and Ag NPs using electrostatic interaction.

XRD was used to characterize the crystal structures and Fig. 2d illustrates the XRD patterns of Fe_3O_4, Fe_3O_4@CoNi LDH and Fe_3O_4@CoNi LDH@Ag NPs. The diffraction peaks at 2θ values of 30.36°, 35.68°, 43.44°, 57.34° and 62.86° can be indexed to the (220), (311), (400), (420) and (440) lattice planes of the Fe_3O_4 structure, respectively.[26] The Fe_3O_4@CoNi LDH shows the typical main reflection planes of (006), (009) and (110) of the LDH material, indicating the formation of the identical hierarchical LDH structure.[27] In addition, the (220), (311), (420), and (440) reflection planes of the typical Fe_3O_4 can be identified. The Fe_3O_4@CoNi LDH material displayed the typical peaks of LDH and Fe_3O_4. Compared to the pure Fe_3O_4@CoNi LDH, the Fe_3O_4@CoNi LDH@Ag NPs exhibited extra diffraction peaks at 38.1°, 64.48° and 77.36°, which are related to the (111), (220) and (311) planes of Ag (JCPDS: 4-0783), respectively.[28] This indicates that the Fe_3O_4@CoNi LDH@Ag NPs were successfully prepared *via* the simple electrostatic self-assembly method.

The composition and element valence of the Fe_3O_4@CoNi LDH@Ag NPs were characterized by XPS. The XPS survey spectrum in Fig. 2e showed the presence of Fe 2p, Co 2p, Ni 2p, Ag 3d, O 1s, and C 1s peaks, further supporting the apparent presence of Fe, Co, Ni, Ag, O, and C elements in the Fe_3O_4@CoNi LDH@Ag NPs, respectively. The XPS spectra of Co, Ni, Fe, and Ag are shown in Fig. S1.† As shown in Fig S1a and b,† the peaks of Co 2p (796.08/780.38) and Ni 2p (855.38/872.78 eV) and other satellite peaks are assigned to the $2p_{3/2}$ and $2p_{1/2}$ orbitals

of Co^{2+} and Ni^{2+}, respectively.[29] Fig. S1c† confirms that the peaks of Fe at 722.68 and 710.98 eV correspond to the Fe $2p_{3/2}$ and Fe $2p_{1/2}$ orbitals, respectively, indicating the presence of complex valence states of iron in this substrate.[30] Furthermore, the peaks of Ag $3d_{3/2}$ and Ag $3d_{5/2}$ appeared at 368.08 and 374.08 eV, respectively, proving that the Ag loaded on the substrate is metallic silver (Fig. S1d†).[31]

Because magnetism plays an important role in separation, the magnetic strength of the Fe_3O_4@CoNi LDH@Ag NPs was tested, and the results are presented in Fig. 2f. No coercivity or remanence was shown in the curves, indicating that all these materials have remarkable magnetic properties and can be separated well in the presence of a magnet. The magnetization saturation value of Fe_3O_4 is 71.3 emu g^{-1}, and with the growth of CoNi LDH and Ag layers, the values for Fe_3O_4@CoNi LDH and Fe_3O_4@CoNi LDH@Ag NPs decreased to 14.6 and 13.6 emu g^{-1}, respectively. Although the magnetism of Fe_3O_4@CoNi LDH@Ag NPs is much lower than that of the Fe_3O_4 nanoparticles, the rapid aggregation of Fe_3O_4@CoNi LDH@Ag NPs in a water system can be completed within 1 min using a permanent hand-held magnet (as depicted in the inset of Fig. 2f). Therefore, the generated magnetic Fe_3O_4@CoNi LDH@Ag NP SERS substrate can offer not only greater adsorption performance for enriching organic dyes, but also efficient magnetic field-assisted separation of the analyte from interfering matrices.[32]

3.2 Optimization of preparation conditions of Fe_3O_4@CoNi LDH@Ag NPs

The SERS performance of the Fe_3O_4@CoNi LDH@Ag NP substrate was influenced by various parameters, including the amount of Fe_3O_4, volume of $Ni(NO_3)_2$, and self-assembly time. Thus, the preparation conditions for the Fe_3O_4@CoNi LDH@Ag NP SERS substrate were optimized by using R6G (1×10^{-6} mol L^{-1}) as the probe molecule.

Firstly, the effect of the Fe_3O_4@CoNi LDH@Ag NPs prepared with different amounts of Fe_3O_4 (1.5, 2.5, 3.5, 4.5, and 5.5 mg) on the intensity of R6G signal was investigated. The intensity of the characteristic peaks of R6G exhibited a progressive increase as the amount of Fe_3O_4 increased from 1.5 to 2.5 mg, as depicted in Fig. 3a and b. In contrast, the intensity of the characteristic peaks of R6G gradually weakened with a further increase in the amount of Fe_3O_4 from 2.5 mg to 5.5 mg. Subsequently, the SERS intensity reached the maximum when the amount of Fe_3O_4 was 2.5 mg. The amount of Fe_3O_4 could tweak the morphology and the physicochemical properties of the obtained Fe_3O_4@CoNi LDH@Ag NP structure. As the Fe_3O_4 content increased, the availability of the Co^{2+} source decreased, hence restricting the amount of ZIF-67 that could be sustained on the magnetic surface. Also, this led to the further growth of a small amount of Ag NPs, hence obtaining weaker SERS signals. Therefore, 2.5 mg Fe_3O_4 was selected to prepare the Fe_3O_4@CoNi LDH@Ag NP SERS substrate.

In this study, the as-prepared ZIF-67 was used as a sacrificial template to prepare LDHs with a specific morphology. The Co^{2+} exposed on the surface of ZIF-67 and Ni^{2+} in the solution reacted with hydroxyl to generate an etched Fe_3O_4@CoNi LDH composite.[33] The $Ni(NO_3)_2 \cdot 6H_2O$ dosage was crucial for tuning the morphology of the final product. Therefore, the effect of the Fe_3O_4@CoNi LDH@Ag NPs prepared with different volumes of $Ni(NO_3)_2 \cdot 6H_2O$ solution (65, 85, 105, 125, and 145 μL) on the SERS intensity of R6G was investigated, and the results are shown in Fig. 3c and d. It is evident that the SERS intensity of

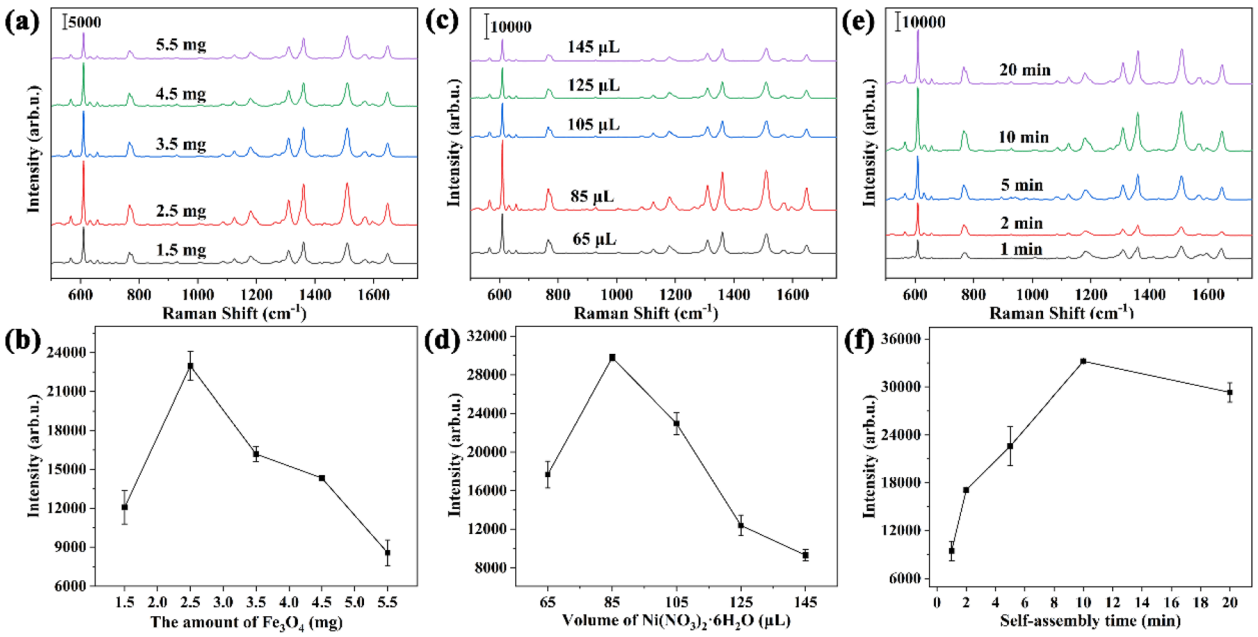

Fig. 3 (a) SERS spectra and (b) SERS intensity line chart at 612 cm^{-1} of R6G (1×10^{-6} mol L^{-1}) on the Fe_3O_4@CoNi LDH@Ag NP substrate with different amounts of Fe_3O_4; (c) SERS spectra and (d) SERS intensity line chart at 612 cm^{-1} of R6G (1×10^{-6} mol L^{-1}) on the Fe_3O_4@CoNi LDH@Ag NP substrate with different volumes of $Ni(NO_3)_2 \cdot 6H_2O$; and (e) SERS spectra and (f) SERS intensity line chart at 612 cm^{-1} of R6G (1×10^{-6} mol L^{-1}) on the Fe_3O_4@CoNi LDH@Ag NP substrate with different self-assembly times.

R6G increased as the volume of $Ni(NO_3)_2 \cdot 6H_2O$ increased from 65 μL to 85 μL. When the volume of $Ni(NO_3)_2 \cdot 6H_2O$ was 85 μL, the SERS intensity reached the maximum, and then diminished as the volume continued to increase. The possible reasons for this are that insufficient content of $Ni(NO_3)_2 \cdot 6H_2O$ did not completely etch Fe_3O_4@ZIF-67, which led to only a small number of Ag NPs adsorbed through electrostatic interactions, hence obtaining weaker SERS signals. However, with an excess volume of $Ni(NO_3)_2 \cdot 6H_2O$, the structure of ZIF-67 may be fractured and even broken into scattered nanosheets, which may lead to a decrease in the SERS properties of the Fe_3O_4@CoNi LDH@Ag NP substrate. Therefore, 85 μL of $Ni(NO_3)_2 \cdot 6H_2O$ solution was selected to be the appropriate volume for preparing the Fe_3O_4@CoNi LDH@Ag NP substrate.

The local plasmon resonance impact of the Ag NPs is crucial for the enhanced SERS properties of the Fe_3O_4@CoNi LDH@Ag NP substrate, which means that the self-assembly time has a greatly impact on its SERS response. Therefore, the effect of different self-assembly times (1, 2, 5, 10, and 20 min) on the properties of the Fe_3O_4@CoNi LDH@Ag NP substrate was studied. As shown in Fig. 3e and f, the intensity of the distinctive peaks of R6G increased progressively as the self-assembly duration increased from 1 min to 10 min, and the highest R6G SERS signal when the self-assembly times was 10 min. Thereafter, as the duration of self-assembly continued to increase, the SERS intensity decreased. This may be because the Ag NPs gradually agglomerated with an extension of the self-assembly time, resulting in fewer "hot spots" and further reducing the SERS intensity. Therefore, the optimal self-assembly time was determined to be 10 min.

3.3 SERS performance evaluation

To study the effect of the LDH shells on the SERS enhancement, the SERS activity of Fe_3O_4, Fe_3O_4@ZIF-67, Fe_3O_4@CoNi LDH, Ag NPs, Fe_3O_4@ZIF-67@Ag NPs, and Fe_3O_4@CoNi LDH@Ag NPs was investigated using R6G as the target molecule (10^{-6} mol L^{-1}), and the results are shown in Fig. 4a. Obvious Raman characteristic peaks related to the R6G appeared for the Ag NPs, Fe_3O_4@ZIF-67@Ag NPs and Fe_3O_4@CoNi LDH@Ag NP substrate, while almost no SERS signals were observed for the Fe_3O_4, Fe_3O_4@ZIF-67, and Fe_3O_4@CoNi LDH substrates. This could be explained by the fact that the Ag NPs were essential in initiating the SERS activity. Furthermore, the SERS performance of the Ag NP substrate was compared with the SERS sensitivity of Fe_3O_4@ZIF-67@Ag NPs and Fe_3O_4@CoNi LDH@Ag NPs. It was discovered that Fe_3O_4@CoNi LDH@Ag NPs and Fe_3O_4@ZIF-67@Ag NPs both exhibited greater SERS enhancements than Ag NPs. The SERS enhancement benefited from the inclusion of absorbent media to enhance the adsorption capacity of the substrates for the target compounds. It was also found that Fe_3O_4@CoNi LDH@Ag NPs exhibited a greater SERS enhancement than Fe_3O_4@ZIF-67@Ag NPs, and the enhancement factor (EF) was calculated to be 5.81×10^8 (see the ESI† for calculation details). Therefore, the CoNi-LDH modification on the Fe_3O_4 surface is important for the SERS detection of the analyte. After Ni^{2+} etching, ZIF-67 was removed and CoNi-LDH nanoshells were formed, and thus Ag NPs were evenly and

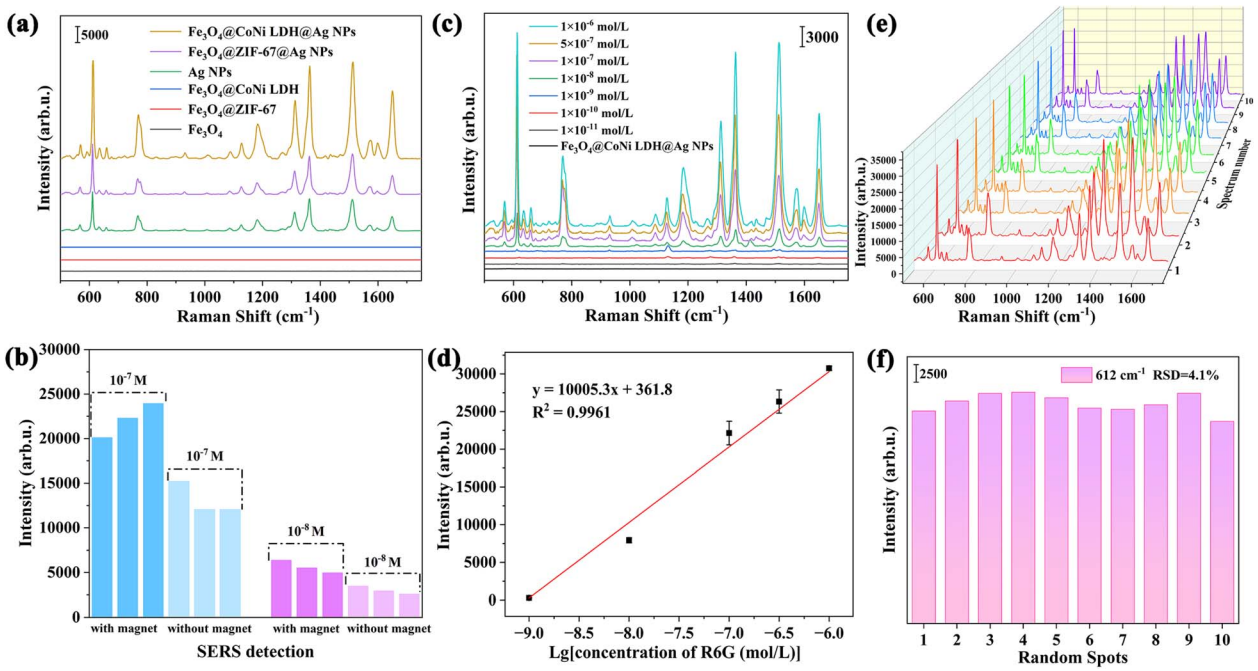

Fig. 4 (a) SERS spectra of different substrates; (b) SERS intensity of R6G (1×10^{-7} and 1×10^{-8} mol L^{-1}) at 612 cm^{-1} obtained at two concentrations by randomly selecting 3 points with or without a magnet; (c) SERS spectrum of R6G at different concentrations (from 1×10^{-11} to 1×10^{-6} mol L^{-1}); (d) calibration curve for logarithmic fitting between the R6G concentration and SERS intensity at 612 cm^{-1}; (e) SERS spectra of 1×10^{-6} mol per L R6G recorded from 10 randomly selected spots on the Fe_3O_4@CoNi LDH@Ag NP substrate; and (f) peak intensity distribution at 612 cm^{-1}.

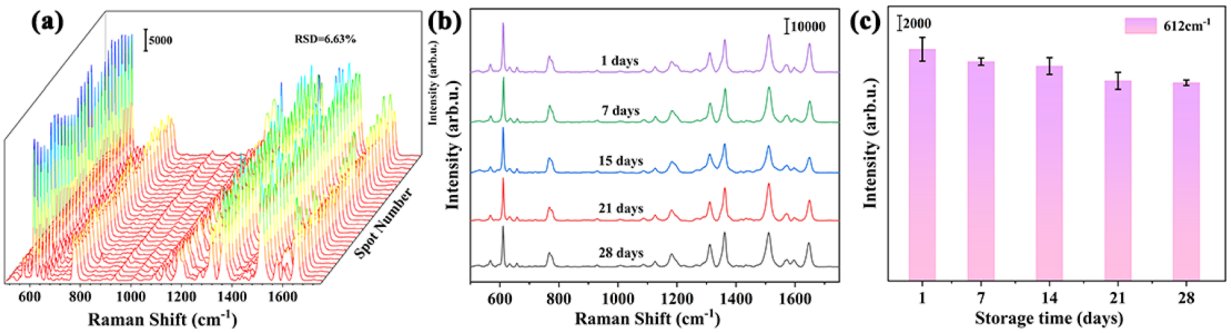

Fig. 5 (a) Reproducibility for R6G detection by Fe_3O_4@CoNi LDH@Ag NP substrate; (b) SERS spectra of 1×10^{-6} mol per L R6G on the Fe_3O_4@CoNi LDH@Ag NP substrate recorded every 7 days; and (c) storage time on the SERS response of the Fe_3O_4@CoNi LDH@Ag NP substrate toward R6G (mol L^{-1}) at 612 cm^{-1}.

firmly loaded on the surface, resulting in abundant "hot spots", which improved the Fe_3O_4@CoNi LDH@Ag NP SERS enhancement.

To verify the effect of an external magnetic field, the SERS intensity of R6G on the Fe_3O_4@CoNi LDH@Ag NP substrate was compared with or without using a magnet (Fig. 4b). Three points were randomly selected to calculate the intensity of the peak (612 cm^{-1}) of R6G in the presence and absence of a magnetic field, respectively. With the aid of a magnetic field, the Fe_3O_4@CoNi LDH@Ag NPs adsorbed with analytes could be quickly enriched, resulting in the average SERS intensity of 1×10^{-7} mol per L R6G increasing from 13 121 to 22 142 a.u. The same tendency was found in the detection of 1×10^{-8} mol per L R6G, where the characteristic peak intensity increased from 3041 to 5649 a.u. The intensity of the SERS signal could be increased by applying a magnetic field during detection. The results showed that the superparamagnetic characteristic of the Fe_3O_4@CoNi LDH@Ag NPs played an important role. The Ag NPs were densely distributed because of the action of the magnetic field, which further formed more "hot spots", resulting in a stronger SERS-enhanced signal.

Sensitivity is a key parameter used to assess the performance of SERS substrates. Thus, to assess the sensitivity of the Fe_3O_4@CoNi LDH@Ag NP substrate, the substrate was mixed with different concentrations of R6G solution (10^{-11}–10^{-6} mol L^{-1}), and then subjected to SERS assay analysis. The SERS spectra in Fig. 4c demonstrated a decrease in R6G intensity as the concentration decreased. However, even when the concentration decreased to 1×10^{-11} mol L^{-1}, the characteristic peak of R6G at 612 cm^{-1} was still observed. At a signal-to-noise ratio of 3 (S/N = 3), the corresponding limit of detection (LOD) was 1×10^{-11} mol L^{-1}. Fig. 4d demonstrates the linear relationship between the SERS intensity at 612 cm^{-1} and the logarithmic concentration of R6G. The linear regression equation can be defined as $y = 10\,005.3x + 361.8$ ($R^2 = 0.9961$). Thus, this result suggests that the created SERS substrates exhibited excellent sensitivity.

Additionally, uniformity and replicability are other essential factors to consider when evaluating the practicality of an SERS substrate. To authenticate the uniformity of the Fe_3O_4@CoNi LDH@Ag NP substrate, 10 spots were chosen at random on the substrate for detecting R6G (1×10^{-6} mol L^{-1}), as seen in Fig. 4e. The histogram generated from the intensity of the characteristic peak at 612 cm^{-1} is shown in Fig. 4f. The relative standard deviation (RSD) was only 4.1%, which demonstrates that the substrate exhibits excellent consistency and can be used as a dependable SERS substrate. Meanwhile, the Raman spectra of R6G (1×10^{-6} mol L^{-1}) were recorded from 30 points randomly selected from 5 batches of Fe_3O_4@CoNi LDH@Ag NP substrates. As depicted in Fig. 5a, the SERS intensity of R6G at 612 cm^{-1} exhibited an average RSD value of 6.63%, which showed that the Fe_3O_4@CoNi LDH@Ag NPs had good reproducibility. For the SERS detection, one limitation of employing simple Ag sols for quantitative measurement is their

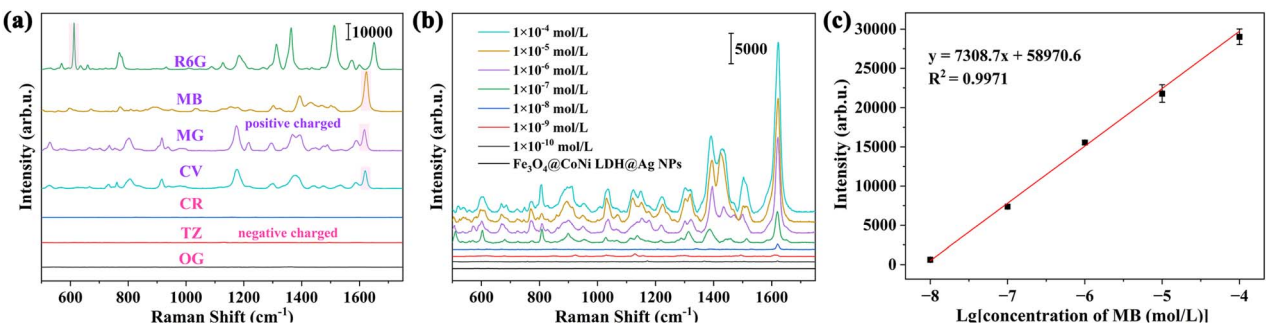

Fig. 6 (a) SERS spectra of cationic dyes (R6G, MB, MG and CV) and anionic dyes (CR, TZ and OG) at the concentration of 10^{-5} mol L; (b) SERS spectra of MB standard solutions with different concentrations (1×10^{-10} to 1×10^{-4} mol L^{-1}); and (c) calibration curve for logarithmic fitting between the MB concentration and SERS intensity at 1623 cm^{-1}.

Table 1 Comparison of SERS substrates used for the analysis of MB

Substrate	Linear range (mol L^{-1})	Correlation coefficient	Limit of detection (LOD)	Enhancement factor	Reference
Fe_3O_4/GO/Ag microspheres	1×10^{-9}–1×10^{-6}	0.91	1×10^{-9}	2.26×10^{7}	31
Paper-based Au/AgNP	3.9×10^{-8}–1×10^{-5}	—	3.9×10^{-8}	9×10^{7}	36
Ag@Fe_3O_4	1×10^{-10}–1×10^{-7}	0.997	3×10^{-10}	1.107×10^{7}	37
Ni$(OH)_2$/Ag	1×10^{-8}–1×10^{-5}	0.97	1×10^{-8}	7.6×10^{5}	38
Fe_3O_4@CoNi LDH@Ag NPs	1×10^{-8}–1×10^{-4}	0.9971	1×10^{-10}	5.81×10^{8}	This work

uncontrollable agglomeration, which would seriously impact the substrate reproducibility. In our case, the Ag NPs were uniformly distributed on the surface of Fe_3O_4@CoNi LDH, which ensured the reproducibility of the material.

To evaluate the stability of the Fe_3O_4@CoNi LDH@Ag NP substrate, the SERS spectra of R6G were recorded every 7 days. As depicted in Fig. 5b and c, the SERS performance of the substrate could maintain good stability for 28 days. After 14 days of storage, the SERS intensity of R6G did not decrease significantly. By the 28th day, the peak intensity of R6G at 612 cm^{-1} decreased only by 14.5%. These results indicate that the Fe_3O_4@CoNi LDH@Ag NP SERS substrate exhibited excellent long-term stability. This may be due to the fact that the unique flower-like structure of the Fe_3O_4@CoNi LDH@Ag NP substrate can improve the stability of Ag NPs. In summary, the Fe_3O_4@CoNi LDH@Ag NP substrate had good detection sensitivity, reproducibility, and long-term stability.

3.4 Selectivity of Fe_3O_4@CoNi LDH@Ag NP substrate

The overuse of organic dyes will cause huge pollution to the water environment, and long-term exposure to these contaminants may cause severe damage to humans, such as deformed babies and carcinogenic effects. Thus, further research was conducted using seven dye molecules as representative dyes to examine the SERS response of the Fe_3O_4@CoNi LDH@Ag NP substrate, including cationic dyes (R6G, MB, MG and CV) and anionic dyes (CR, TZ and AO), at a concentration of 10^{-5} mol L^{-1}. Fig. 6a displays a comparison of the SERS intensity. It is evident that the SERS signals of the cationic dye molecules (R6G, MB, MG and CV) were significantly higher than that of the anionic dye molecules, indicating that the magnetic Fe_3O_4@CoNi LDH@Ag NP substrate could generate higher SERS signals for the detection of these cationic dyes. In contrast, no SERS enhancement was detected for anionic dye molecules (CR, TZ and AO) on the Fe_3O_4@CoNi LDH@Ag NP substrate. The results showed that the Fe_3O_4@CoNi LDH@Ag NP substrate exhibited strong SERS enhancements for cationic dye molecules of R6G, MB, MG and CV with high sensitivity and selectivity. This may be attributed to the negative zeta potential of Fe_3O_4@CoNi LDH@Ag NPs of −11.87 mV (Fig. 2c), which could selectively adsorbed dye molecules with the opposite charge *via* electrostatic interaction, and then enhance their Raman signal. In addition, the adsorptive property of Fe_3O_4@CoNi LDH@Ag NPs also was influenced by the structure of the dye molecules.[34] Therefore, the SERS signals intensity of MG and CV were weaker than that of R6G and MB because of their bigger size. These finding demonstrated that the proposed Fe_3O_4@CoNi LDH@Ag NPs could be regarded as an SERS substrate with high sensitivity for the selective detection of cationic dyes in real-world scenarios.

3.5 SERS analysis of MB by Fe_3O_4@CoNi LDH@Ag NPs

For the further evaluation of the detection sensitivity of the SERS method, the Fe_3O_4@CoNi LDH@Ag NP substrate was used for the detection of different concentrations (10^{-10}–10^{-4} mol L^{-1}) of MB standard solution. As shown in Fig. 6b, the major Raman peaks of MB at 602, 1395, and 1623 cm^{-1} are assigned to the C–H in-plane ring deformation, C–S–C backbone deformation, and C–C ring stretching vibration, while the characteristic peaks at 895, 1038, and 1152 cm^{-1} are generated by the C–H in- and out-of-plane bending vibration, respectively.[35] The intensity of the distinctive peaks of MB decreased gradually with a decrease in its concentration in the range of 10^{-10}–10^{-4} mol L^{-1}. The intensity of Raman peaks decreased with the reduction of MB concentration from 1×10^{-4} to 1×10^{-10} mol L^{-1}. However, the SERS signal of MB could still be clearly detected even at a concentration as low as 1×10^{-10} mol L^{-1}. This result confirms that the SERS performance of the Fe_3O_4@CoNi LDH@Ag NP substrate was excellent. As shown in Fig. 6c, the intensity of the peak at 1623 cm^{-1} showed a good linear correlation with the logarithmic concentration of MB in the range of 10^{-8}–10^{-4} mol L^{-1}. The calibration curve was $y = 7308.7x + 58\,970.6$ with R^2 of 0.9971. The corresponding LOD value for MB was 1×10^{-10} mol L^{-1}.

Table 2 Recoveries of MB in environmental water showing the applicability of Fe_3O_4@CoNi LDH@Ag NPs ($n = 3$)

Sample	Spiked level (mol L^{-1})	Recovery (%)	RSD (%)
Snow water	0	—	—
	1×10^{-5}	96.74	8.61
	1×10^{-6}	103.72	5.52
	1×10^{-7}	93.53	6.82
Rain water	0	—	—
	1×10^{-5}	97.90	9.59
	1×10^{-6}	95.40	9.16
	1×10^{-7}	90.11	10.0
Lake water	0	—	—
	1×10^{-5}	97.45	3.87
	1×10^{-6}	97.18	10.26
	1×10^{-7}	89.68	9.07

The SERS performances of the Fe_3O_4@CoNi LDH@Ag NPs were compared with that of other reported substrates for the detection of MB. As shown in Table 1, the Fe_3O_4@CoNi LDH@Ag NP substrate exhibited a greater EF value, lower LOD, and more advantageous linear range compared to the SERS approach that was previously described. To validate the feasibility of Fe_3O_4@CoNi LDH@Ag NPs as an SERS substrate, environmental water samples of snow water, rainwater, and lake water were used for the analysis of MB. MB was not detected in all the environmental water samples. Thus, spiked recovery experiments of MB were performed in the environmental water samples. As shown in Table 2, the recoveries of MB in the three environmental water samples were between 89.68% and 103.72% with RSD values of less than 10.26%. Thus, the results revealed that the Fe_3O_4@CoNi LDH@Ag NP SERS substrate possesses significant prospect for the detection MB in environmental monitoring.

4. Conclusions

In this study, a spherical flower-like magnetic Fe_3O_4@CoNi LDH@Ag NP SERS substrate was successfully produced using an electrostatic self-assembly method, which was applied for the sensitive and rapid detection of cationic dyes in environmental water samples. The Ag NPs were uniformly and densely immobilized on the surface of Fe_3O_4@CoNi LDH, and thus produced numerous of "hot spots". The Fe_3O_4@CoNi LDH@Ag NPs with negatively charged surface appeared as hierarchical structures, which could not only rapidly adsorb trace amounts of dye molecules, but also effectively enrich cationic dye molecules to "hot spots" through electrostatic interactions, and thus showed higher SERS sensitivity to cationic dyes. The substrate exhibited an extraordinary SERS performance with good homogeneity (RSD = 4.1%), ultra-low LOD of 1×10^{-11} mol L^{-1}, sustained stability for a minimum duration of 28 days, and enhancement factor of 5.8×10^8. Meanwhile, the substrate showed an excellent detection performance for MB, with recoveries ranging from 89.68% to 103.72% and RSD values of less than 10.26%. Thus, it is anticipated that the as-prepared Fe_3O_4@CoNi LDH@Ag NP substrate can be beneficial for the ultrasensitive detection of cationic dyes with strong application potential in environment safety assurance.

Data availability

The authors confirm that the data supporting the findings of this study are available within the article and its ESI.†

Author contributions

Shuxian Ren: investigation, writing original draft. Jihong Fu: data curation, conceptualization, validation. Guoqi Liu: methodology. Haipeng Zhang, Boshen Wang, Junli Yu: verifying information.

Conflicts of interest

There are no conflicts to declare.

Acknowledgements

This work was supported by the Natural Science Foundation of Xinjiang Uygur Autonomous Region [2020D01C032] and the National Natural Science Foundation of China [No. 21565024].

References

1 S. Khan, T. Noor, N. Iqbal and L. Yaqoob, *ACS Omega*, 2024, **9**, 21751–21767.
2 A. Majeed, A. H. Ibrahim, S. S. Al-Rawi, M. A. Iqbal, M. Kashif, M. Yousif, Z. U. Abidin, S. Ali, M. Arbaz and S. A. Hussain, *ACS Omega*, 2024, **9**, 12069–12083.
3 I. Khan, K. Saeed, I. Zekker, B. Zhang, A. H. Hendi, A. Ahmad, S. Ahmad, N. Zada, H. Ahmad, L. A. Shah, T. Shah and I. Khan, *Water*, 2022, **14**, 242.
4 R. Ahmadi, G. Kazemi, A. M. Ramezani and A. Safavi, *Microchem. J.*, 2019, **145**, 501–507.
5 M. R. Khan, M. A. Khan, Z. A. Alothman, I. H. Alsohaimi, M. Naushad and N. H. Al-Shaalan, *RSC Adv.*, 2014, **4**, 34037–34044.
6 X. Huang, G. Yang, Y. Tang and L. Wang, *Chemosensors*, 2024, **12**, 52.
7 C. Tian, L. Zhao, J. Zhu and S. Zhang, *J. Hazard. Mater.*, 2021, **416**, 126251.
8 Y.-F. Li, C.-J. Zou, X.-B. Liu, F. Gan and P.-P. Fang, *Anal. Chem.*, 2023, **95**, 7933–7940.
9 H. Yilmaz, D. Yilmaz, I. C. Taskin and M. Culha, *Adv. Drug Delivery Rev.*, 2022, **184**, 114184.
10 B. Li, S. Liu, L. Huang, M. Jin and J. Wang, *Coord. Chem. Rev.*, 2023, **494**, 215349.
11 M. A. Badshah, J. Kim, J. Yeom, N. Abbas, M. R. Haq, Y. Kim, X. Lu and S.-M. Kim, *Appl. Surf. Sci.*, 2021, **542**, 148587.
12 J. Langer, D. Jimenez de Aberasturi, J. Aizpurua, R. A. Alvarez-Puebla, B. Auguié, J. J. Baumberg, G. C. Bazan, S. E. J. Bell, A. Boisen, A. G. Brolo, J. Choo, D. Cialla-May, V. Deckert, L. Fabris, K. Faulds, F. J. García de Abajo, R. Goodacre, D. Graham, A. J. Haes, C. L. Haynes, C. Huck, T. Itoh, M. Käll, J. Kneipp, N. A. Kotov, H. Kuang, E. C. Le Ru, H. K. Lee, J.-F. Li, X. Y. Ling, S. A. Maier, T. Mayerhöfer, M. Moskovits, K. Murakoshi, J.-M. Nam, S. Nie, Y. Ozaki, I. Pastoriza-Santos, J. Perez-Juste, J. Popp, A. Pucci, S. Reich, B. Ren, G. C. Schatz, T. Shegai, S. Schlücker, L.-L. Tay, K. G. Thomas, Z.-Q. Tian, R. P. Van Duyne, T. Vo-Dinh, Y. Wang, K. A. Willets, C. Xu, H. Xu, Y. Xu, Y. S. Yamamoto, B. Zhao and L. M. Liz-Marzán, *ACS Nano*, 2020, **14**, 28–117.
13 Q. Yang, D.-W. Sun and H. Pu, *Trends Food Sci. Technol.*, 2023, **141**, 104202.
14 J. Singh, R. K. Soni, D. D. Nguyen, V. Kumar Gupta and P. Nguyen-Tri, *Chemosphere*, 2023, **339**, 139735.

15 H. T. Ali, A. Mateen, F. Ashraf, M. R. Javed, A. Ali, K. Mahmood, A. Zohaib, N. Amin, S. Ikram and M. Yusuf, *Ceram. Int.*, 2021, **47**, 27998–28003.
16 J. Yang and Y.-W. Yang, *Small*, 2020, **16**, 1906846.
17 B. Ge, J. Huang, H. Qin, S. Zhao, F. Yang, M. Wang and P. Liang, *Microchim. Acta*, 2024, **191**, 308.
18 F. Xu, W. Shang, M. Xuan, G. Ma and Z. Ben, *Chemosphere*, 2022, **288**, 132635.
19 Y. Dong, X. Kong, X. Luo and H. Wang, *Chemosphere*, 2022, **303**, 134685.
20 Z. Zhao, Q. Zhao, L. Zhou, Y. Wei, B. Lei, H. Zhang and W. Cai, *J. Hazard. Mater.*, 2023, **459**, 132156.
21 F. Yang, Y. Gong, M. Zhou, X. He, L. Niu, C. Li and X. Liu, *Appl. Surf. Sci.*, 2023, **612**, 155701.
22 H. Deng, X. Li, Q. Peng, X. Wang, J. Chen and Y. Li, *Angew. Chem., Int. Ed.*, 2005, **44**, 2782–2785.
23 Y. Sun and Y. Xia, *Science*, 2002, **298**, 2176–2179.
24 J.-P. Wei, B. Qiao, W.-J. Song, T. Chen, F. li, B.-Z. Li, J. Wang, Y. Han, Y.-F. Huang and Z.-J. Zhou, *Anal. Chim. Acta*, 2015, **868**, 36–44.
25 Y. Liu, X. Teng, Y. Mi and Z. Chen, *J. Mater. Chem. A*, 2017, **5**, 24407–24415.
26 L. Chen, Y. He, Z. Lei, C. Gao, Q. Xie, P. Tong and Z. Lin, *Talanta*, 2018, **181**, 296–304.
27 G. Li, X. Zhang, J. Sun, A. Zhang and C. Liao, *J. Hazard. Mater.*, 2020, **381**, 120985.
28 H. Yang, Q. He, M. Lin, L. Ji, L. Zhang, H. Xiao, S. Li, Q. Li, X. Cui and S. Zhao, *J. Hazard. Mater.*, 2022, **435**, 129082.
29 D. Xu, M. Muhammad, L. Chu, Q. Sun, C. Shen and Q. Huang, *Anal. Chem.*, 2021, **93**, 8228–8237.
30 T. Yamashita and P. Hayes, *Appl. Surf. Sci.*, 2008, **254**, 2441–2449.
31 J. He, G. Song, X. Wang, L. Zhou and J. Li, *J. Alloys Compd.*, 2022, **893**, 162226.
32 Z. Sun, J. Du, L. Yan, S. Chen, Z. Yang and C. Jing, *ACS Appl. Mater. Interfaces*, 2016, **8**, 3056–3062.
33 X. Qiao, X. Chen, C. Huang, A. Li, X. Li, Z. Lu and T. Wang, *Angew. Chem., Int. Ed.*, 2019, **58**, 16523–16527.
34 X. Xie, X. Huang, W. Lin, Y. Chen, X. Lang, Y. Wang, L. Gao, H. Zhu and J. Chen, *ACS Omega*, 2020, **5**, 13595–13600.
35 I. Shaikh, M. A. Haque, H. Pathan and S. Sartale, *Plasmonics*, 2022, **17**, 1889–1900.
36 G. Yang, X. Fang, Q. Jia, H. Gu, Y. Li, C. Han and L.-L. Qu, *Microchim. Acta*, 2020, **187**, 310.
37 V.-T. Hoang, L. T. Tufa, J. Lee, M. Q. Doan, N. H. Anh, V. T. Tran and A.-T. Le, *J. Alloys Compd.*, 2023, **933**, 167649.
38 X. Wen, H. Cheng, W. Zhang, L. You and J. Li, *Talanta*, 2024, **266**, 125140.